Status of ARGO-YBJ: an overview

M. Iacovacci[a] for the ARGO-YBJ Collaboration

[a]INFN and University of Napoli,
Complesso Universitario MSA, Via Cintia, 80126 Napoli, Italy

Within a Collaboration Agreement between INFN and CAS (Chinese Academy of Science), the ARGO-YBJ experiment is completely installed at the YangBaJing Cosmic Ray Laboratory (4300 m a.s.l., Tibet, P.R. China). ARGO-YBJ is a plane detector, with a total detection area of ~ 6500 m^2, made of Resistive Plate Chambers (RPCs) which provide a detailed space-time picture of the charged component of the extensive air showers. At present the detector is completely mounted and the central carpet of 5800 m^2 is operating under a multiplicity trigger $N_{pad} \geq 20$, the trigger rate is about 3.5kHz and the data flow is 5MB/s. A 0.5 cm lead converter will be mounted on the detector in the summer 2007.

1. Detector

The ARGO [1] apparatus consists of a full coverage array of dimension 77.85×74.5 m^2 made of a single layer of Resistive Plate Counters (RPCs), 2.80×1.25 m^2 each [2]. The percentage of active area in the carpet is $\sim 93\%$. A guard ring surrounding, the central carpet up to 109.5×98.5 m^2, is partially ($\sim 20\%$) instrumented with RPCs. A 0.5 cm thick lead converter will uniformly cover the detector in order to improve the angular resolution. The basic DAQ unit is the cluster, a set of 12 contiguous RPCs (5.7×7.6 m^2). Each chamber is read by 80 strips of 6.75 x 61.8 cm^2, logically organized in 10 independent pads of 55.6 x 61.8 cm^2, which are individually acquired and represent the time granularity of the detector. The digital read-out of the RPCs, performed by means of strips, well suited to detect small size air showers, implies a limitation to the measurable energy of a few hundreds of TeV. In order to extend the measurable energy range, each RPC has been equipped with two large size pads of dimensions 1.40 x 1.25 m^2 [3]. These electrodes, called "BigPad", provide a signal whose amplitude is expected to be proportional to the charged particles impinging on the detector. Presently the RPCs are operated in streamer mode, with a gas mixture of Argon (15%), IsoButhane (10%) and R134a (75%). The operating voltage is 7.2 kV. This setting provides a typical efficiency of 95% with a time resolution better than 1 ns and a m.i.p. signal on the Big-Pad of ~ 1.7 mV. The analog readout system is in operation on 1080 m^2 (24 clusters) of the detector, allowing a cross-check of digital and analog information.

The detector is operated at the same time both in shower mode, that means the position and the time of each fired pad is recorded when the trigger condition is satisfied, and in scaler mode (SPT), that means the particle coincidences of ≥ 1, ≥ 2, ≥ 3 and ≥ 4, happening in a time window of 150 ns, are read in each cluster every 500 ms. The measured rates for ≥ 1, ≥ 2, ≥ 3 and ≥ 4 particles are, respectively, 40 kHz, 2 kHz, 300 Hz and 120 Hz for each cluster [4,5].

1.1. Data Taking

From December 2004 till June 2005, 42 clusters covering 1900 m^2 - about 1/3 of the central carpet - have been operated continuously. The data acquisition has run for more than 2140 hours. About 7 TB data were acquired, i.e. about 2×10^9 cosmic ray events were recorded. The trigger condition required more than 60 fired pads. The event rate was about 160 Hz. Then there was another data taking with 104 clusters, it lasted about 4 months starting from February 2006. Presently the central carpet, that is 130 clusters for 5800 m^2, is in continuous data taking with a multiplicity trigger of $N_{pad} \geq 20$; the trigger rate

is 3.5 kHz and the data flow is 5Mb/s as expected. The results reported here essentially refer to the first data set.

2. γ-Astronomy

In a search for astrophysical point sources with ground-based detector arrays the angular resolution is certainly fundamental as well as a firm way to calibrate the detector . The shadowing effect of the cosmic rays made by the Moon, along with using the Earth's magnetic field as a magnetic spectrometer, can be exploited both to measure the angular resolution and to perform an absolute calibration of the energy scale. However, a large sample of events is necessary to obtain a statistically significant result since the intensity reduction is small. Another approach is to rely on consistency checks between data and MC calculations.

2.1. Angular Resolution

An estimate of the pointing accuracy of the detector has been made [6] through the ψ_{72} parameter, defined as the opening angle which contains $\sim 72\%$ of the events in the angular distribution. Assuming that the Point Spread Function (PSF) of the detector is Gaussian, it represents the angle which maximizes the signal/noise ratio for a point source on an uniform background. In the above approximation the angular resolution of the detector is given by the relation $\sigma \approx \psi_{72}/1.58$. In Fig.1 the opening angle ψ_{72}, estimated from data via the chessboard method, is compared to the MC simulation as a function of the pad multiplicity N_{pad} (sum of even and odd pads). To this aim, proton-induced showers have been simulated with a primary energy spectrum $E^{-2.75}$, with E ranging from 100 GeV to 1 PeV in the uniform zenith angle interval $0° \leq \theta \leq 40°$. The upper scale shows the estimated median energy of proton-induced and triggered events in the different multiplicity bins. As it can be seen from the plots, there is a satisfactory agreement of the simulated result with the experimental one. The ψ_{72} parameter is found to be roughly proportional to $N_{pad}^{-0.7}$. At low multiplicity the poor agreement between data and MC is due to the high contami-

nation of external events, that means events with the core outside the detector. We expect the lead to improve significantly ($> 30\%$) the angular resolution even at low multiplicity [7]. In the MC events the angular resolution can be computed directly from the differences $\Delta\theta_{true/rec}$ between true and reconstructed shower directions; in Fig.1 the filled circles refer to the parameter ψ_{72} calculated in this way. The worsening of the opening angle at very large shower sizes, is probably related to a similar worsening in the shower core determination. We notice that there is a full consistency between MC and data when the chessboard method is applied to both, therefore we conclude that, for the ARGO-42 data and without any lead, the estimated angular resolution is $1.1°$ at a median energy of about 4 TeV.
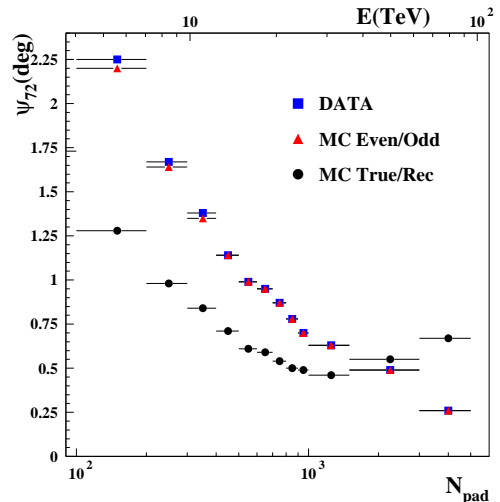

Figure 1. The opening angle ψ_{72} estimated by the Chessboard Method both for the ARGO-42 data and MC simulations, as a function of pad multiplicity. The same quantity is reported for MC simulations when the difference $\Delta\theta_{true/rec}$ is considered (see text) . The zenith angle of selected events is $\theta \leq 40°$. The error bars refer to the width of the pad multiplicity bins.

2.2. Moon Shadow

Although preliminarily, the moon shadow has been observed [8] in the data with 42 clusters in two independent analyses. The data correspond to about 330 hours of moon observation,

at $\theta \leq 50°$. In order to estimate the background, the equi-zenith angle method has been used: the number of events has been averaged over 6 off-source windows of the same size as the on-source one, at the same zenith angle and in the same time interval of the on-source window. This method eliminates the systematic effects caused by changes in pressure and temperature of the atmosphere. Results are preliminary and refinements are in progress. In Fig.2 the moon shadow is reported. The maximum significance, 4.9 σ, is found at 0.7° west and 0.5° north with a 1.5° smoothing radius. The same smoothing radius reproduces the deficit as function of time. The
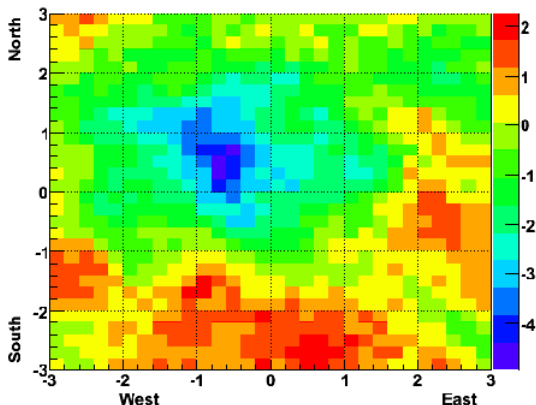

Figure 2. Preliminary sky map of ARGO-42 around the Moon position for $N_{pad} \geq 60$ and $\theta \leq 50°$. The scale on the right indicates the statistical significance in each $0.2° \times 0.2°$ bin.

estimated angular resolution is 1.2° and we quote this value as angular resolution of the ARGO-42 carpet, quite in agreement with the MC expectation which is about 1.1° . In order to understand systematic effects like the unexpected shift toward north, further studies are in progress while statistics is increasing and we are looking for better cuts to clean our data sample.

3. GRB Search

ARGO-YBJ is able to cover the energy range 1-100 GeV by working in scaler mode; due to the high altitude location and the large detection area (~ 6500 m^2), this experiment is the most sensitive among all present and past ground-based detectors. A search for GRBs in coincidence with satellite detections has been performed for the period December 2004 - August 2006 [4] when the ARGO detector was in a heavy mounting phase, therefore the data refer to different areas. The search for emission from GRBs started with the first GRB detection by the Swift satellite on December 17, 2004, when only 16 clusters ($\sim 1/10$ of the total surface) were in data taking. Only satellite events within the ARGO field of view with $\theta \leq 40°$ have been considered. Table 1 reports the list of such GRBs along with the results. No excess has been found so far in coincidence with satellite detection; the 3 σ fluence upper limits have been calculated in the 1-100 GeV energy range using the spectral indices measured by satellites. When the redshift is known, a model for the Extragalactic Background Light (EBL) absorption has been adopted [9], otherwise z=0 (no absorption) was assumed. We notice that, with the above assumptions, they are the lowest limits obtained in this energy range by all ground-based detectors.

4. Cosmic Rays

4.1. Cosmic Ray Spectrum below 100 TeV

The strip size spectrum (N_s) has been measured by using the RPC digital readout [10]. Working under digital readout mode, each induction strip serves as a shower particle counter. A preliminary study of the strip size spectrum up to $N_s=10^4$, which is due to primary cosmic rays with energies up to about 100 TeV, has been performed. The composition models provided by JACEE [12] and RUNJOB [11] have been considered. These two balloon-born experiments obtained data up to hundreds of TeV, although they suffer from statistics for E > 100 TeV. Apart from the importance related to the helium content of the primary radiation [17,16] , this energy region is interesting because represents a 'bridge' between direct and indirect measurements [16].

The preliminary results are shown in Fig.3, where only statistical errors are reported. Therefore without a careful check of systematic errors,

Table 1
List of GRBs with zenith angle $\theta \leq 40°$ (December 2004 - August 2006), with corresponding 3σ fluence upper limits.

GRB	Sat.	T90/Dur. (s)	θ^* (deg)	Redshift	Spectral Index	Carpet Area (m^2)	$n_\sigma^§$	UL† (Fluence)
041228	Swift	62	28.1	–	1.56	693	-0.34	$5.8 \cdot 10^{-4}$
050408	HETE	15	20.4	1.24	1.98	1820	-1.2	$\mathbf{1.1 \cdot 10^{-4}}$
050509A	Swift	12	34.0	–	2.1	1820	0.44	$1.8 \cdot 10^{-4}$
050528	Swift	11	37.8	–	2.3	1820	-0.03	$6.2 \cdot 10^{-4}$
050802	Swift	13	22.5	1.71	1.55	1820	0.82	$\mathbf{8.5 \cdot 10^{-5}}$
051105A	Swift	0.03	28.5	–	1.33	3379	-1.5	$1.3 \cdot 10^{-5}$
051114	Swift	2	32.8	–	1.22	3379	1.2	$2.5 \cdot 10^{-5}$
051227	Swift	8	22.8	–	1.31	3379	-0.89	$2.1 \cdot 10^{-5}$
060105	Swift	55	16.3	–	1.11	3379	1.3	$1.6 \cdot 10^{-4}$
060111A	Swift	13	10.8	–	1.63	3379	-0.54	$3.4 \cdot 10^{-5}$
060115	Swift	142	16.6	3.53	1.76	4505	0.17	$\mathbf{1.2 \cdot 10^{-3}}$
060421	Swift	11	39.3	–	1.53	4505	-0.71	$1.9 \cdot 10^{-4}$
060424	Swift	37	6.7	–	1.72	4505	-0.05	$7.6 \cdot 10^{-5}$
060427	Swift	64	32.6	–	1.87	4505	-0.39	$4.1 \cdot 10^{-4}$
060510A	Swift	21	37.4	–	1.55	4505	2.0	$3.4 \cdot 10^{-4}$
060526	Swift	14	31.7	3.21	1.66	4505	0.63	$\mathbf{1.5 \cdot 10^{-4}}$
060717	Swift	3	7.4	–	1.72	5632	1.08	$1.3 \cdot 10^{-5}$
060801	Swift	0.5	16.8	–	0.47	5632	0.10	$4.8 \cdot 10^{-6}$
060807	Swift	34	12.4	–	1.57	5632	0.61	$7.6 \cdot 10^{-5}$

∗ Zenith angle.
§ Significance of the signal for the single event.
† Upper Limits on the fluence (1 – 100 GeV) in erg cm^{-2}. The numbers in bold take into account absorption by the EBL.

although there is a preference for the RUNJOB model, no firm conclusion can be drawn. The ability of this result to favour one of the two models relies on the capability to keep systematic errors below 10%.

4.2. Forbush Decrease on January 2005

The SPT data from 15th to 27th of January 2005, after air pressure correction, are used to search for the Forbush Decrease (FD) that is well measured by devices at lower energies such as neutron monitors. The FD around noon on January 17, 2005 has been observed by the ARGO detector (Fig.4). The SPT rates with multiplicity greater than 1 and 2 clearly decrease correspondingly [13]. All detailed structures of the light curves are similar to the results from neu-

tron monitors. The maximum amplitudes of the FD are about -5% and -4%, respectively. The SPT rates of multiplicities greater than 3 and 4 show no signs of decrease.

4.3. Lateral distribution near the core at high energies

A measurement of the lateral distribution of the charged particles in the shower, near the core region, has been performed with data taken in the period February-April 2006 when 24 clusters were operated with the analog readout. The ADC scale was set to 0-20 V [3]. Only vertical showers ($\theta < 20°$) with the core inside a fiducial area of the 24 clusters have been considered. The selected events have been classified according to the maximum ADC count. Three ranges of the
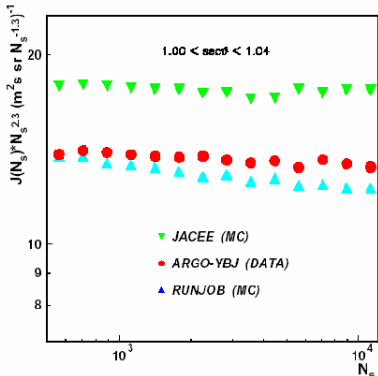
Figure 3. The ARGO-YBJ strip size spectrum as compared with the expected ones, namely with the RUNJOB and JACEE composition models (see text).

Figure 4. Counting rates summed up for 12 clusters in ARGO-YBJ from January 15th to 27th , 2005

ADC maximum count (Amp_{max}) have been defined, namely: $50 < Amp_{max} < 500$, corresponding to a mean energy $< E > \sim 500$ TeV and a maximum density $\rho_{max} \sim 500$ part./m^2; $500 < Amp_{max} < 3000$, with $< E > \sim 1000$ TeV and $\rho_{max} \sim 2000$ part./m^2; finally $3000 < Amp_{max} < 4000$ with $< E > \sim 5000$ TeV and $\rho_{max} \sim 10000$ part./m^2. In Fig.5 the result is reported . The geometry and the selection criteria (internal events) allow to measure up to ~ 20 m from the core. The result is compared with a very naive model of composition, namely 50% protons and 50% iron. Systematic errors come from calibration and assumption of linear behavior of the RPC, moreover no change in the primary composition has been taken into account. Although simple, this result shows the potentiality of the detector in the shower physics field and confirms that ARGO-YBJ is able to perform γ-astronomy above 10 TeV and cope with the cosmic ray composition around the knee region [14].

4.4. Inelastic Cross Section Measurement of σ_{p-Air} and σ_{p-p}

The decrease of the shower frequency with the zenith angle, when considered at fixed primary energy and shower age, gives a measure of the flux attenuation at that energy [15]. Such a flux a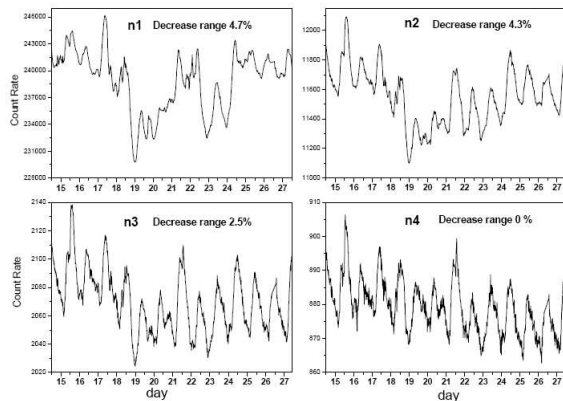ttenuation is controlled by the absorption length Λ which is related to the interaction length. Thus, in principle, from Λ we can estimate the p-Air and p-p cross sections. An analysis of this kind has been performed on a small set of the 42 cluster data by using the digital readout . Two sub-samples of events have been defined with mean energy of 3.67 and 14.3 TeV respectively; the corresponding values obtained for σ_{p-Air} are (273 ± 15) mb and (289 ± 20) mb [18]. The results are reported in Fig.6 and, although preliminary, they are in fair agreement with other measurements. Under specific assumptions the total σ_{p-p} has been inferred, obtaining the results of (39 ± 4) mb and (44 ± 5) mb at the two energies. They are still in good agreement with the other measurements. These results suggest a promising extension to unexplored energy regions, thanks to the analog readout.

5. Conclusions

ARGO-YBJ has been completely mounted. The central carpet (5800 m^2) is in data taking since July 2006, the guard ring will be put in data acquisition quite soon. The lead plates (0.5 cm) will be put on the detector in the summer 2007. In this configuration we expect to see the Crab signal in about 3 months at energies
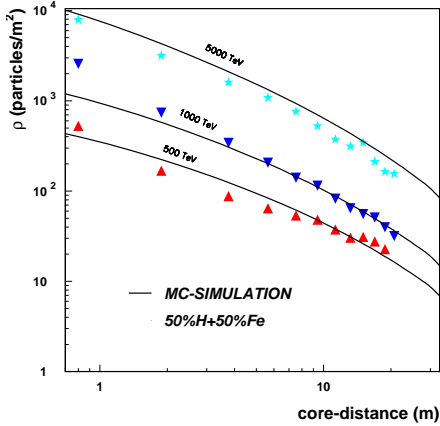
Figure 5. Preliminary measured lateral distributions in ARGO-YBJ (points) and MC expectations (see text)

of about 1 TeV [19], without any γ-proton discrimination . First estimates of the angular resolution, along with the moon observation, make us confident that ARGO-YBJ will perform efficiently γ-astronomy. The Forbush decrease observation confirms the potentiality of the apparatus with respect to transient phenomena and solar physics. A GRB search in scaler mode has been carried out and, although no evidence for signal has been found till now, the most stringent upper limits have been put. On the cosmic ray side we have preliminary, very interesting and promising results, ranging from the measurements of σ_{p-Air} and σ_{p-p}, to the cosmic ray spectrum (strip size). The analog readout allows to perform γ-astronomy above 10 TeV and to face the cosmic ray composition around the knee region; moreover, thanks to the detector features, it permits to operate near the core in a very interesting kinematical region.

REFERENCES

1. M. Abbrescia et al. (ARGO-YBJ Coll.), Astroparticle Physics with ARGO, Proposal (available at http://argo.na.infn.it), 1996.
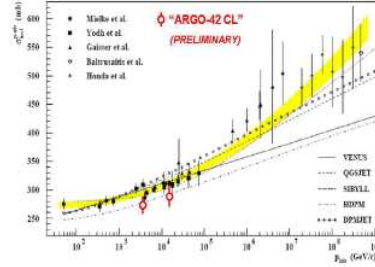2. G. Aielli et al. (ARGO-YBJ Coll.), Nucl. Inst. and Meth. in Phys. Res. A, vol.562, (2006) 92.

Figure 6. Inelastic cross section σ_{p-Air} preliminarily measured with a data sample of ARGO-42 (open circles) as compared with other measurements and theoretical estimates.

3. P. Creti et al. (ARGO-YBJ Coll.), 29th ICRC, Pune 8, (2005) 97.
4. P. Vallania et al., 20th ECRS, Lisbon (2006), in press.
5. F. R. Zhu et al., these proceedings.
6. G. Di Sciascio et al., 20th ECRS, Lisbon (2006), in press.
7. C. Bacci et al., Astrop. Phys. 17, (2002) 151.
8. Y. Wang et al., these proceedings.
9. T.M. Kneiske et al., A&A 413, (2004) 807.
10. L. Saggese et al., 29th ICRC, Pune 6, (2005) 37.
11. A.V. Apanasenko et al., Astropart. Phys.16, (2001) 13.
12. K. Asakimori et al., Astrophys. Journ. 502, (1998)278.
13. H.Y. Jia et al., 29th ICRC, Pune 1, (2005) 137.
14. M. Zha et al., these proceedings.
15. J. Alvarez-Muniz et al., Phys. Rev. D 66, (2002) 123004.
16. E.S. Seo et al., these proceedings.
17. T. K. Gaisser et al., 27th ICRC, Hamburg, (2001) 1643.
18. A. Surdo et al., 20th ECRS, Lisbon (2006), in press.
19. S. Vernetto et al., 28th ICRC, Tsukuba (2003), 3007.